EC4MACS

Uncertainty Treatment

The CHIMERE Atmospheric Model

European Consortium for Modelling of Air Pollution and Climate Strategies - EC4MACS

Editors:
Debry, Edouard
Malherbe, Laure

Issued by: INERIS

March 2012

Content

Summary

This report was done in the frame of the EC4MACS project (EU LIFE) to determine the urban increment to be used in the GAINS calculations.

Sighted pollutants were mainly ozone (O_3) during summer and particles during winter. For these latest the PM_{10} indicator is used. A Monte Carlo methodology has been implemented, which enables to propagate the uncertainty of input parameters into the model, thus getting the uncertainty of predicted concentrations.
This report focuses on urban areas, as nowadays population living in cities (especially mega-cities) over the world has outnumbered that of rural areas. Urban areas are distinguished thanks to the GLCF land use and the population density spreading out.
Main results delivered in this study are estimations for absolute and relative uncertainty of both sighted pollutants, and the list of input parameters to which they are the most sensitive.

The average absolute and relative uncertainty for O_3 are respectively 16 $\mu g.m^{-3}$ and 21%. Relative uncertainty is mainly driven by the concentration level, decreasing with it, so that relative uncertainty is the lowest on peaks. It doest not change significantly between urban areas.
The average absolute and relative uncertainty for PM_{10} concentrations are respectively 4 $\mu g.m^{-3}$ and 17%. Conversely to O_3, relative uncertainty depends not only on concentration level, slightly reduced on high pollution events, but also on urban area.

According to the sensitivity analysis, notorious illustrative parameters for both pollutants are temperature and deposition velocities. Illustrative parameters peculiar to O_3 concentrations are boundary conditions and chemical reaction rates, whereas those peculiar to PM_{10} concentrations are fine carbon emissions and specific humidity.
The large influence of temperature and boundary conditions on ozone and PM10 concentrations confirm that the impact of emission projections has to be assessed in the context of global changes.

1 Introduction

1.1 Issues at stake

Dispersion models are nowadays widely and often used not only to inform the public at large of the pollution level, but also to assess the efficiency of regulatory actions and perform impact studies around industrial plants.
These operating processing make modeling engineers evaluate the quality of their predictions and warn end users of how confident they are with simulations on which decision-makers rely. Simulated concentrations are indeed only an approximation of the true concentrations, for physical processes are usually given a simplified representation in dispersion models, hence uncertainty. Chemistry transport models are also used to develop an integrated strategy to optimize the emission reduction in Europe.
In the framework of its support activities for the MEEDDM[1], INERIS has been developing the Prev'Air ([5]) platform which delivers daily predictions for ozone, PM_{10} and nitrogen dioxide up to two days ahead. CHIMERE is also used in the frame of the EC4MACS[2] project (EU LIFE) to calculate the urban increment in the integrated assesment of emission control strategies.

The goal of this study is to quantify uncertainty associated with predicted concentrations and to determine which parameters contribute the most to it, with a focus on the most populated areas. The study will focus on a domain centered on France, this region being representative of urban diversity in Europe.

1.2 Modeling uncertainties

One may first identify several levels of uncertainties by going through the dispersion model principles.
A dispersion model relies on the numerical integration of an transport-diffusion-reaction equation. This one is written as follows for the concentration c_i of one pollutant X_i (e.g. O_3) :

$$\frac{\partial c_i}{\partial t} + \mathrm{div}(Vc_i) = \mathrm{div}(\rho K \nabla \frac{c_i}{\rho}) + \chi_i(c) + S_i - P_i \qquad (1)$$

This equation depends on several parameters : the wind speed V, the air density ρ, the diffusion tensor K, the production and loss by chemical reactions between pollutants $\chi(c)$, emissions S_i, and deposition processes P_i.
These parameters are either raw data (emissions, wind speed) or estimated data thanks to physical parametrization and experimental measurements.
Thus uncertainty may arise from :

[1] French Ministry for Ecology, Energy, Sustainable Development and Sea
[2] European Consortium for Modelling of Air Pollution and Climate Strategies

1. raw data, that is to say input fields, among which mainly emissions, boundary conditions, and meteorological fields,
2. physical parametrization, which usually constitute the core of the model,
3. numerical schemes for integrating equation (1).

That is to note the three levels are prone to significant uncertainties, up to a factor of 2 for biogenic emissions ([4]). In the sequel we do not take into account of numerical schemes for they are usually hard-coded in dispersion models.

Eq. 1 stands for a deterministic model where one given value (or field value) is attached to each input parameter. Assessing uncertainties require to combine such model with a stochastic approach in which the previous values of input parameters represent one possible state among many others. The concentration vector c resulting from integration of Eq. 1 represent from now on one state of a random concentration vector $\hat{c}$.

In this scope, if we label $\bar{c}$ the expected value of $\hat{c}$, the uncertainty of pollutant concentrations is then fully described by the covariance matrix Σ of vector $(\hat{c}-\bar{c})$.
In practice, Σ cannot be fully computed. The uncertainty for one pollutant at a given time and location (labeled i within the vector concentration) is assessed either with the scalar standard deviation, either absolute, $\sqrt{\Sigma_{i,i}}$, or relative, $\frac{\sqrt{\Sigma_{i,i}}}{\bar{c}_i}$.
In the sequel, we will refer to these scalars for assessing uncertainty.

2 Methodology

In this part, we shortly describe the methodology applied to the Chimere model.

2.1 Uncertainty of input parameters

In practice, the stochastic approach implies to attach to each input parameter one probability density function (PDF) which describes the uncertainty of the parameter. The shape of the PDF is most often log-normal (LN) or normal (N), but can also be uniform (U) if there are too poor knowledge on the parameter uncertainty ([7]).
The expected value for each input parameter is taken equal to its current value in the deterministic model. The standard deviation of normal and log-normal PDFs, labeled σ, is the measure of the parameter uncertainty.
In the literature, σ is often given in a more significant form as the 95% confidence interval, which is approximately $2\times\sigma$, or as expressions like ``plus or minus a factor Y'' or ``plus or minus Z %'' ([4]). Relationships $(Y=1+Z/100)$ and $\sigma=0.5\log(Y)$ enables to pass from one to another. [3] Attaching PDFs to input parameters is a difficult task. As an example, table 1 shows

[3] $\log$ denotes the natural logarithm

the various choices made so far in the literature for wind speed.

PDF	PDF coefficient[1]	reference
LN	factor 1.5	[4]
LN	$\pm 1.5\, m.s^{-1}$	[8]
LN	$\pm$ 30%	[3]
N	$\pm$ $1\, m.s^{-1}$	[1]
U	$[0.1\, m.s^{-1}, 8\, m.s^{-1}]$	[7]
LN	$\sigma =$ 0.1 / 1.0 / 2.0	[7]

Table 1: Wind speed PDF in the literature.

The standard deviation is usually derived from measurement uncertainty or expert concerting. For one pollutant, the standard deviation must at least reflect the difference between observation and simulations.
In the framework of this study, we make several restrictions :

- only normal and log-normal PDFs are used,
- when the parameter is a field, say temperature, this one is perturbed once, niformly along space and time,
- input parameters are two by two independent.

The last restriction implies that the joint PDF of all input parameters is simply the PDFs product.

2.2 Propagation of uncertainty in the model

Once PDFs have been assigned to input parameters, the joint PDF has to be propagated into the model so as to obtain the PDF of concentrations. To do so, Monte Carlo methods are generally a good choice, they do not require any assumptions on the model.
The principle of such methods is to perform several random draws for input parameters according to their joint PDF. For each draw one model simulation is done. As draws goes along, the joint PDF of input parameters is better and better sampled and the PDF of concentrations converges.
If we label c_j the concentration vector of j^{th} draw, the expected value and covariance matrix of the concentration vector c after N draws are respectively computed as follows :

$$\bar{c}^N = \frac{1}{N}\sum_{j=1}^{N} c_j \,,\; \Sigma^N = \frac{1}{N}\sum_{j=1}^{N} \Sigma_j \qquad (2)$$

According to the central limit theorem, Monte Carlo methods converge with the inverse square

of draws, $\sqrt{\Sigma}/\sqrt{N}$. The number of draws necessary to reach a given accuracy is all the greater as the variance Σ is important.
This is the drawback of Monte Carlo methods which can be computationally demanding.

2.3 Sensitivity analysis

The goal of sensitivity analysis is to assess the model response to the variation of parameters. A reference simulation is defined and several simulations are performed in which one parameter is varied at a time, all others staying at their reference value. The model response is defined as the deviation to the reference simulation concentrations.
It is then possible to sort parameters according to their sensitivity level by comparing their deviations. This can also be done with Monte Carlo simulations.
If we denote Δp_i^j the relative perturbation of parameter p_i for the j^{th} Monte Carlo simulation, the model response Δc_j can be expressed as one weighted linear combination of parameter perturbations :

$$\Delta c_j = \sum_i \omega_i \Delta p_i + b \tag{3}$$

where b is a constant bias and ω_i[4] is the weight for i^{th} parameter, expressed in the same unit as concentrations.
Each weight ω_i comes with a standard deviation σ_i standing for its own uncertainty. A parameter is said illustrative if the uncertainty of its weight does not exceed 50% of weight value :

$$\frac{\sigma_i}{\omega_i} < 0.5 \tag{4}$$

Illustrative parameters are then those which mainly contribute to the model response. A great weight (in absolute) does not necessarily mean the parameter significantly contributes to the model uncertainty, but that its own uncertainty (input PDF) should be accurately quantified.

3 Chimere Monte Carlo set up

3.1 Simulations

The Chimere Monte Carlo experiment has been run for two periods. The first one, denoted "summer"', runs during 30 days in 2009 from 30^{th} of July to 28^{th} of august included, and second one, labeled "winter", runs during 9 days from 5 to 13^{th} of January 2010 included. The Chimere version used in this study is "2008b". Branchs "gas" and "aerosol" of this version have been used respectively for summer and winter periods.
For each period, boundary conditions are derived from a simulation at a larger scale over a European domain, and initial conditions are taken from a ten days spin-up[5] simulation.

[4]Weights (ω_i) are computed through the Moore-Penrose pseudo-inverse of matrix (Δp_i^j)

[5]Time period after which initial conditions have no more significant influence

The Monte Carlo experiment is carried out by the Polyphemus driver named “incertitude” ([6]) which randomly choose perturbations at the beginning of Chimere simulation and apply them to input parameters after each reading step of Chimere.

3.2 PDFs of input parameters

As PDFs are a key point in Monte Carlo simulations, we detail in the sequel the choice made for each parameter. We refer mainly to [3, 4, 1, 8]. That is to note few data are available up to now for parameters related to particles. We assume that uncertainty for particle parameters is at least greater than that for gas parameters. Table 2 displays the PDF used for meteorological fields.

Field	PDF	factor
meridional wind	LN	1.5
zonal wind	LN	1.5
wind direction	N	20.0
temperature	N	0.01
2 meters temperature	N	0.01
specific humidity	N	0.20
Kz	LN	1.7
precipitation	LN	2.0
attenuation	LN	1.3
liquid water content	LN	2.0

Table 2: Meteorological fields PDFs

That is to note meridional and zonal winds are perturbed with the same random value, so as to keep constant its direction. Then the wind direction is perturbed while keeping its module constant. Table 3 displays PDFs for lateral and top boundary conditions.

pollutant	top		lateral		pollutant	top		lateral	
O3	LN	2.0	LN	1.5	NO	LN	3.0	LN	3.0
NO2	LN	3.0	LN	2.0	SO2	LN	2.0	LN	2.0
OXYL	LN	3.0	LN	3.0	C5H8	LN	3.0	LN	3.0
C2H6	LN	3.0	LN	3.0	APINEN	LN	3.0	LN	3.0
AnA1D	LN	3.0	LN	3.0	AnBmP	LN	3.0	LN	3.0
BiA1D	LN	3.0	LN	3.0	BiBmP	LN	3.0	LN	3.0
PPMaq	LN	3.0	LN	3.0	H2SO4aq	LN	2.0	LN	2.0
HNO3aq	LN	2.0	LN	2.0	NH3aq	LN	2.0	LN	2.0
AnA1Daq	LN	3.0	LN	3.0	AnBmPaq	LN	3.0	LN	3.0
BiA1Daq	LN	3.0	LN	3.0	BiBmPaq	LN	3.0	LN	3.0
SALTaq	LN	3.0	LN	3.0	DUSTaq	LN	3.0	LN	3.0

OCARaq	LN	3.0	LN	3.0	BCARaq	LN	3.0	LN	3.0
pBCAR	LN	3.0	LN	3.0	pDUST	LN	3.0	LN	3.0
pOCAR	LN	3.0	LN	3.0	pPPM	LN	3.0	LN	3.0
pSALT	LN	3.0	LN	3.0	pAnA1D	LN	3.0	LN	3.0
pAnBmP	LN	3.0	LN	3.0	pBiA1D	LN	3.0	LN	3.0
pBiBmP	LN	3.0	LN	3.0	pISOPA1	LN	3.0	LN	3.0
pH2SO4	LN	2.0	LN	2.0	pHNO3	LN	2.0	LN	2.0
pNH3	LN	2.0	LN	2.0	pWATER	LN	2.0	LN	2.0

Table 3: Boundary conditions PDFs

Boundary and initial conditions for particle pollutants are perturbed independently between particle sizes. Table 4 displays PDFs for gas and particle pollutants which have biotic and/or anthropic emission fields.

Anthropic emissions			**Biotic emissions**		
pollutant	**PDF**	**factor**	**pollutant**	**PDF**	**factor**
NO	LN	1.5	NO	LN	2.0
NO2	LN	1.5	C5H8	LN	3.0
OXYL	LN	2.0	APINEN	LN	3.0
C5H8	LN	2.0	DUST mode big	LN	3.0
C2H6	LN	2.0	DUST mode coarse	LN	3.0
APINEN	LN	2.0	DUST mode fin	LN	3.0
SO2	LN	1.5	SALT mode coarse	LN	3.0
H2SO4 mode fin	LN	2.0	Na mode coarse	LN	2.0
PPM mode big	LN	4.0	HCL mode coarse	LN	2.0
PPM mode coarse	LN	4.0	H2SO4 mode coarse	LN	2.0
OCAR mode fin	LN	4.0	WATER mode coarse	LN	2.0
BCAR mode fin	LN	4.0			

Table 4: Emission fields PDFs

There are no estimation for uncertainty of particle carbon emissions to our knowledge. Nevertheless, when looking at the reference simulation for winter period, we noticed the PM_{10} average concentration over stations is 22.4 $\mu g.m^{-3}$, whereas that for observations is 60.5 $\mu g.m^{-3}$. Then, assuming this difference is mainly due to an underestimation of particle carbon emissions, which are indeed usually high because of wood burning, we should choose a factor of 4 to reflect the gap between simulated and observed concentrations.

All chemical reaction rates are independently perturbed with a log-normal PDF. The factor is 1.1, except for reactions listed in table 5 ([1]).

Reactions	**PDF**	**factor**

oRO2 + NO -> NO2 + HO2	LN	1.3
oRO2 + HO2 -> oROOH	LN	1.3
CH3COO + NO -> CH3O2 +	LN	1.2
CH3COO + NO2 + M -> PAN	LN	1.2
PAN + M -> CH3COO + NO2	LN	1.3
O3 -> 2 OH	LN	1.3
NO2 -> NO + O3	LN	1.2
HCHO -> CO + 2 HO2	LN	1.4
HO2 -> 0.5 H2O2	LN	1.3
NO3 -> HNO3	LN	1.3
NO2 -> 0.5 HONO +	LN	1.3
N2O5 -> 2 HNO3	LN	1.3
N2O5 -> 2 HNO3AQ	LN	1.3

Table 5: Chemical reaction rates PDFs

At last, deposition velocities are perturbed with a log-normal shape and factor 1.5.

4 Urban areas

In order to focus on the most populated areas, one has to determine how "urban" is a grid cell. This can be done either according to the land use or the population density spreading out. The land use spreading out is an input parameter field for dispersion models. Chimere uses the GLCF[6] database which provides for each cell the land use apportionment between thirteen land types, among which "urban and built-up".

The space domain of dispersion models is discretized into several cells along latitude and longitude axis. In our case, the Chimere french domain is a regular grid with a resolution of $0.1^\circ \times 0.15^\circ$.

Figures 1 shows respectively the GLCF "urban and built-up" percentage and the population density over the french domain in each grid cell. The GPW[7] database at 1km resolution is used for the population density.

[6] GLCF : Global Land Cover Falicity : http://glcf.umiacs.umd.edu/index.shtml

[7] GPW : Gridded Population of the World : http://sedac.ciesin.columbia.edu/gpw/

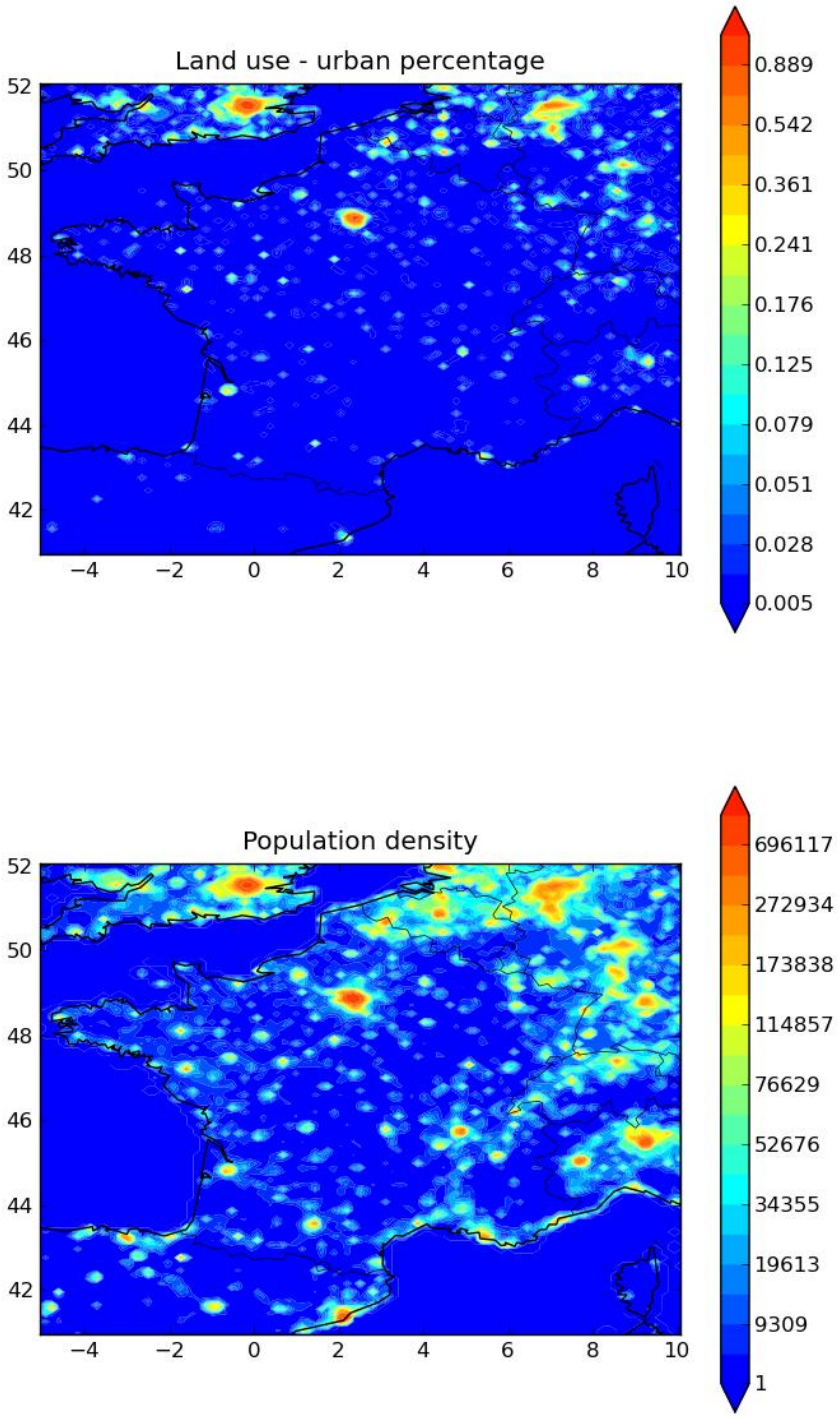

Figure 1: Urban areas according to GLCF land use and population density.

Most of urban areas highlighted by the GLCF database have also a significant population density but the inverse is not true. Nevertheless, as the population density over urban areas in France is

at least greater than 200 km^{-2}, cells with a population greater than 50000 inhabitants should also be taken into account, given the domain resolution.
In order to take into account for both criteria, we select cells whose “urban and built-up” percentage exceeds 60% or whose population exceeds 50000 inhabitants. The selected cells are displayed on figure 2.

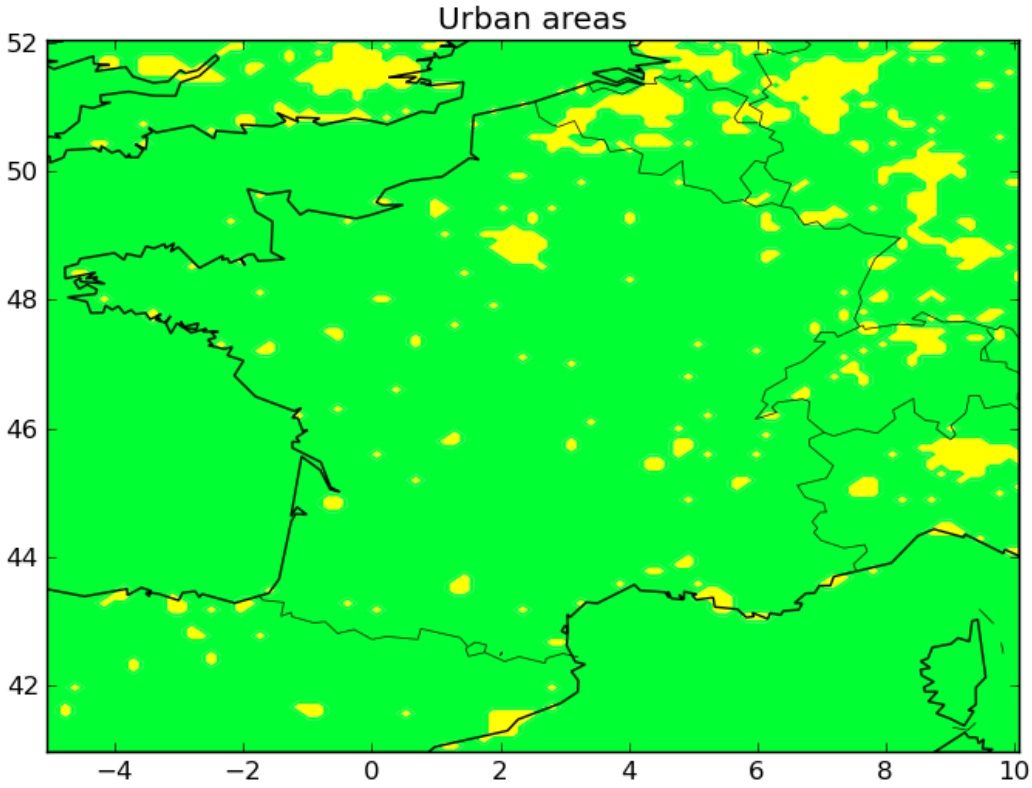

Figure 2: Selected cells for urban areas.

In the sequel, only theses highlighted cells will be used.

5 Uncertainty patterns over urban areas

For summer period, 500 simulations were achieved, and 300 for the winter period. In both cases, the Monte Carlo process reached an accuracy below 1%.
The purpose of this part is to investigate the uncertainty patterns of O_3 concentrations in summer and PM_{10} concentrations in winter. Only hourly concentrations at first height level over urban areas are considered.
First, we display uncertainty maps, then we explore how much uncertainty dispersion is related

to the concentration level and the urban area. At last, we assess the model sensitivity to parameters, some of which may mainly contribute to uncertainty.

5.1 Maps of pollutants

5.1.1 Ozone

Figure 3 displays the time averaged O_3 concentration over the french domain.

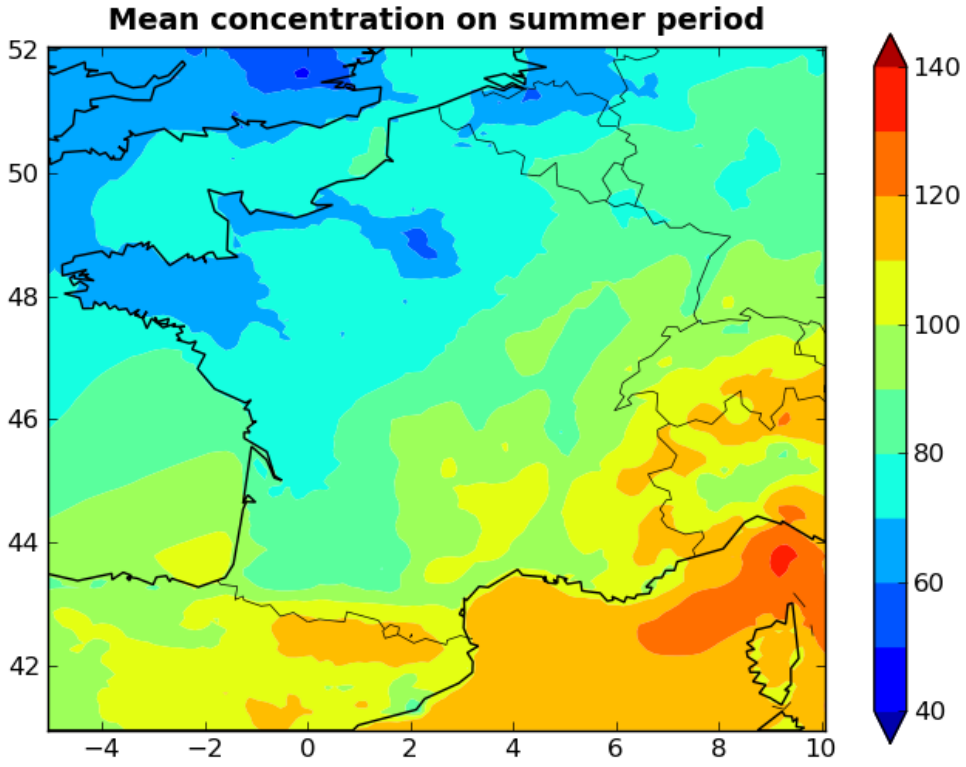

Figure 3: Average O_3 concentration in $\mu g.m^{-3}$

The space averaged concentration over urban areas is 78 $\mu g.m^{-3}$. It is particularly low on mega-cities as Paris and London due to titration effects.
Figures 4 and 5 respectively show the absolute and relative standard deviation for the time averaged concentration.

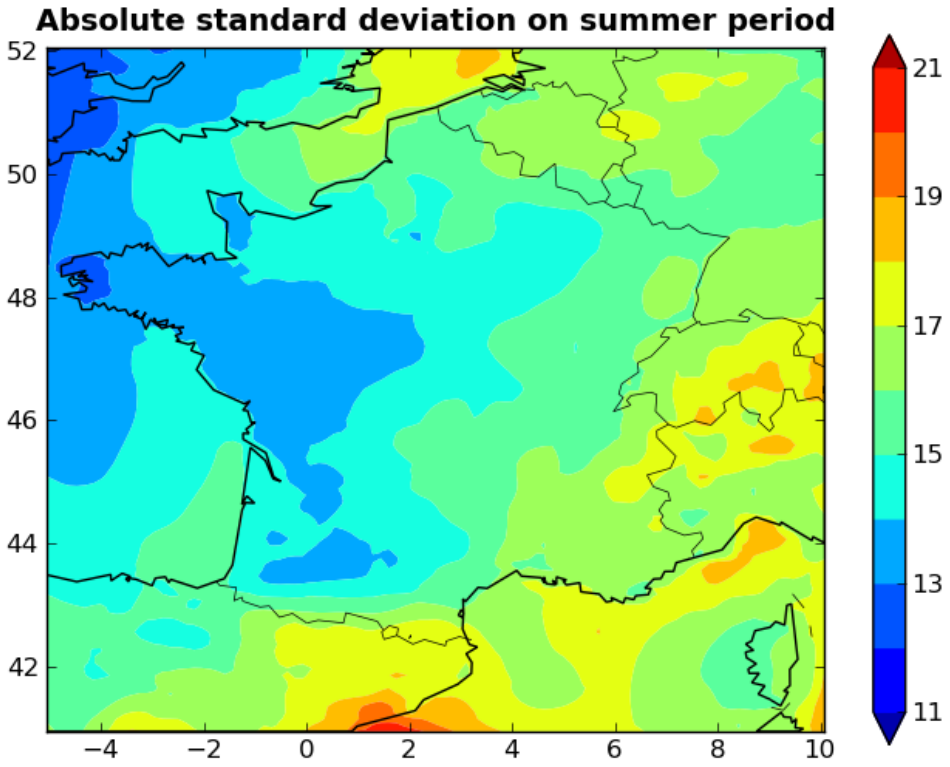

Figure 4: Absolute uncertainty.

The space averaged absolute standard deviation over urban areas is 16 $\mu g.m^{-3}$, whereas that of relative standard deviation is 21%.

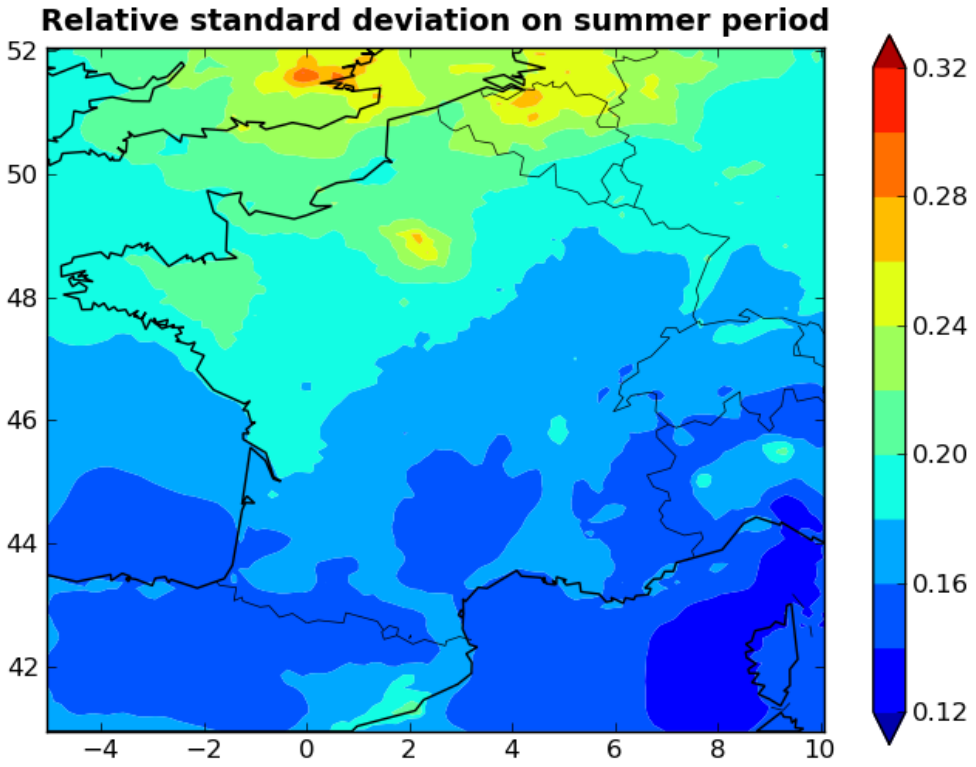

Figure 5: Relative uncertainty

The time averaged concentration and absolute standard deviation tend to be lower over urban areas, whereas urban areas are clearly highlighted by the relative standard deviation.

5.1.2 Particles

Figure 6 displays the time averaged PM_{10} concentration over the french domain.

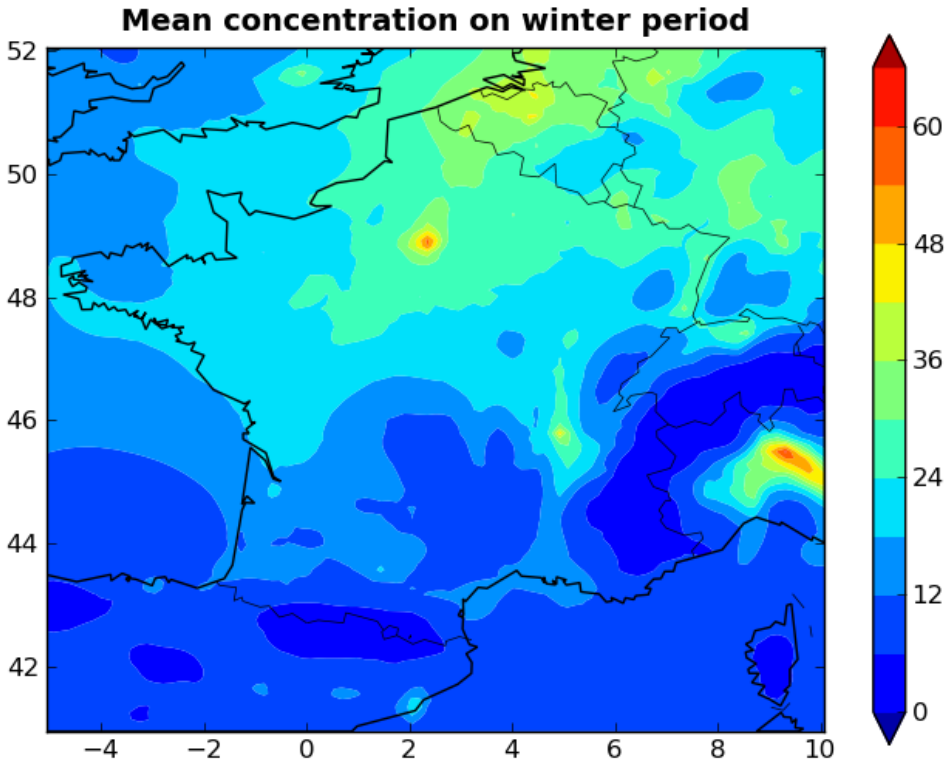

Figure 6: Average PM_{10} concentration on winter period ($\mu g.m^{-3}$)

The average concentration over urban areas is 25 $\mu g.m^{-3}$. One can note the high pollution patterns are located over Paris and the Pô valley. The BeneLux and Rhone-Alpes also show high pollution levels.

Figures 7 and 8 show respectively the absolute and standard deviation for the time averaged concentration.

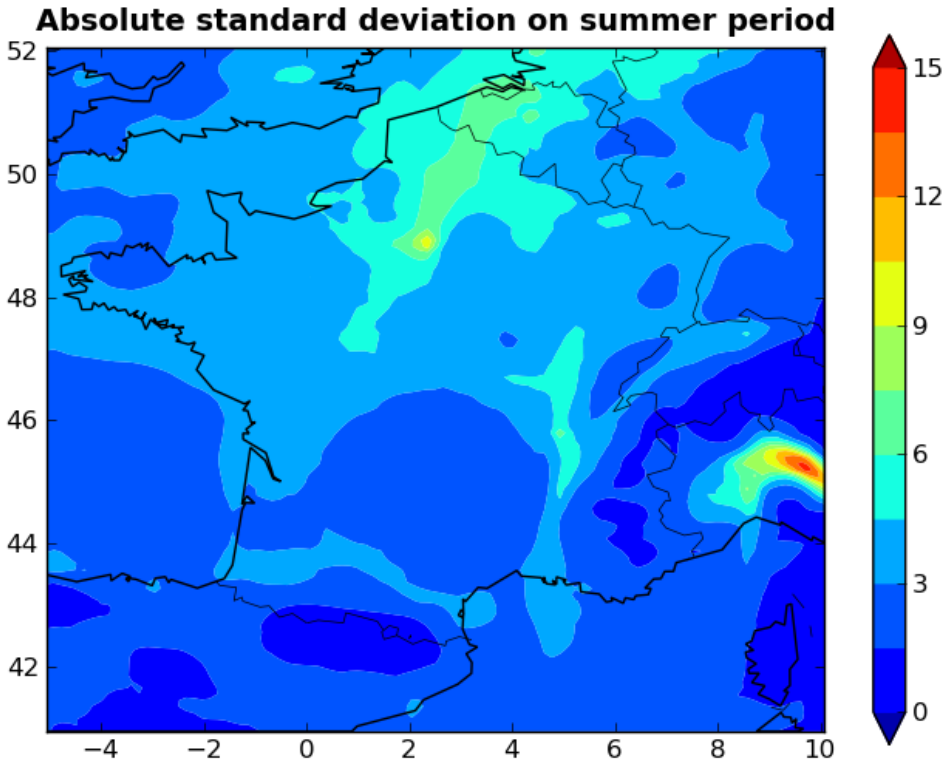

Figure 7: Absolute uncertainty

The space averaged absolute standard deviation over urban areas is equal to 4 $\mu g.m^{-3}$, that of the relative standard deviation is 17%.

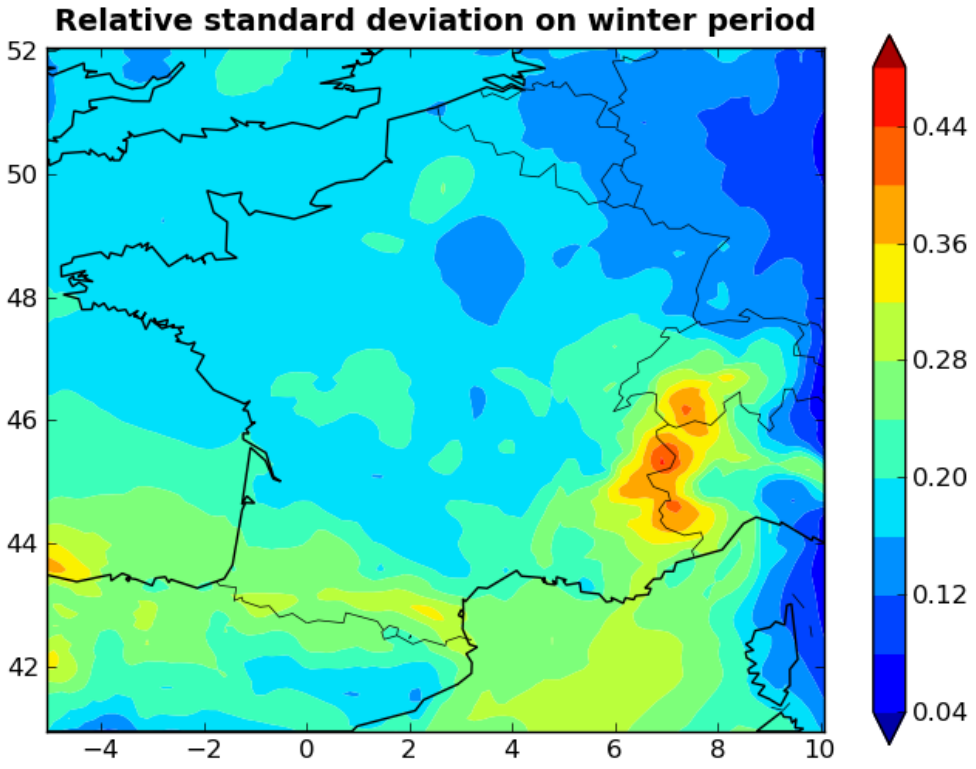

Figure 8: Relative uncertainty.

The relative standard deviation on PM_{10} concentrations tends to be lower over urban areas, for concentrations are often greater on theses. The peaks observed over mountain regions (Alpes and the Pyrenees) are mainly due to very low concentrations.

5.2 Uncertainty dispersion

5.2.1 Ozone

Figures 9 and 10 depict respectively the absolute and relative standard deviation with respect to concentration level. For each figure and concentration level, the average uncertainty is represented as a black square. Within one concentration level, the standard deviation of uncertainty is displayed as a green error bar. As uncertainty values are time averaged, the green error bar only accounts for space dispersion.

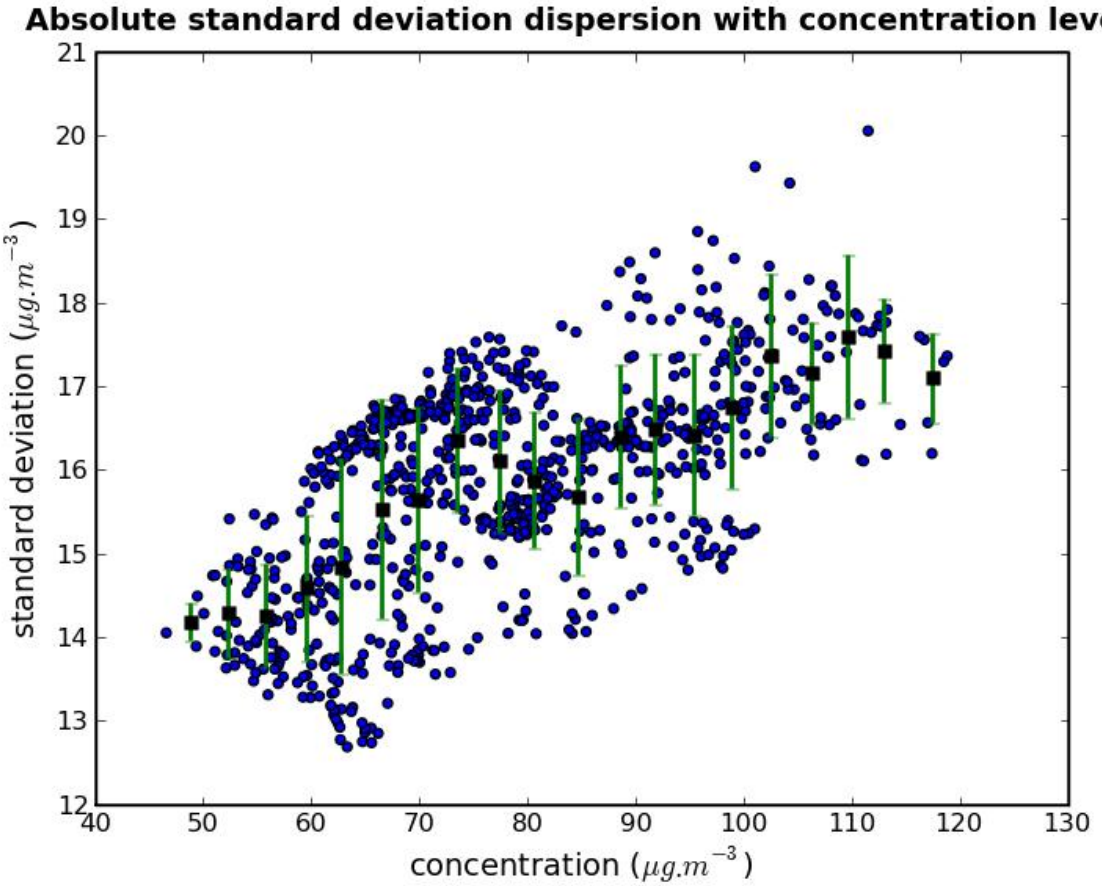

Figure 9: Absolute uncertainty dispersion

Absolute uncertainty and concentration level appear to be correlated (60%), whereas relative uncertainty is anti-correlated, but much strongly (90%) than absolute uncertainty.

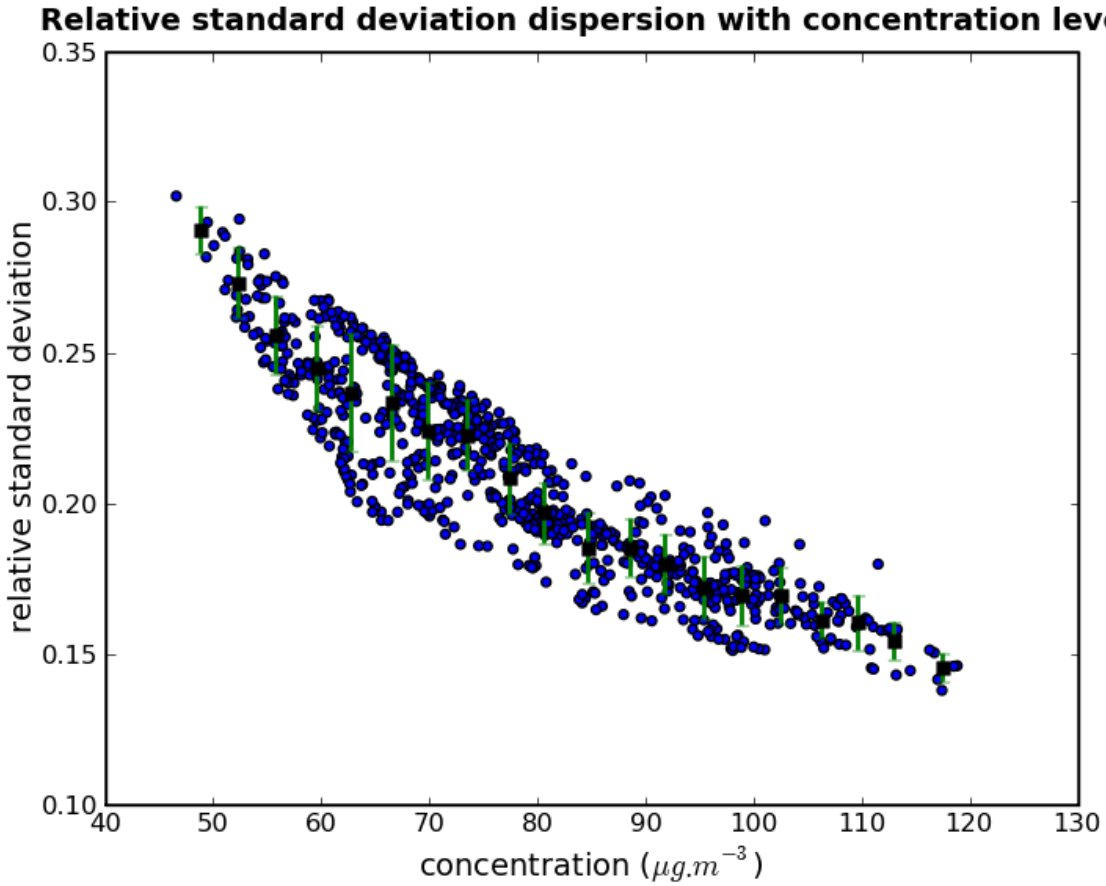

Figure 10: Relative uncertainty dispersion

Absolute uncertainty tends to increase with the concentration level. The standard deviation of absolute uncertainty with concentration level is 1 $\mu g.m^{-3}$, whereas the its standard deviation with space is 0.84 $\mu g.m^{-3}$.

Thus absolute uncertainty for O_3 over urban areas is driven not only by the concentration level but also by their location.

The relative uncertainty, as for it, clearly decreases with the concentration level. Its own standard deviation with the concentration level and space are respectively 4% and 1%. On the contrary to absolute uncertainty, relative uncertainty is mainly driven by the concentration level.

That is to note relative uncertainty is reduced up to 15% for high concentrations, that is to say the so-called O_3 peaks.

5.2.2 Particles

Figures 11 and 12 are respectively equivalent to figures 9 and 10 for PM_{10} concentrations.

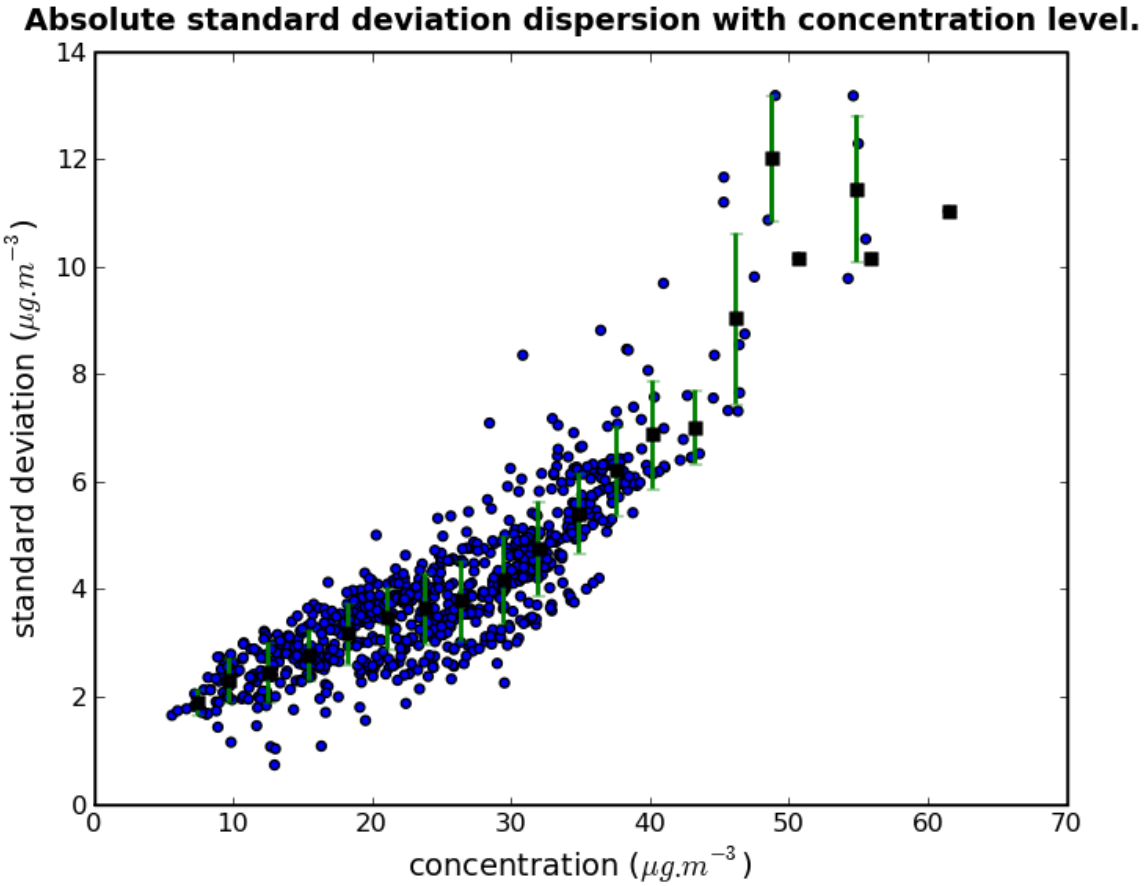

Figure 11: Absolute uncertainty dispersion.

Absolute uncertainty is strongly (85%) correlated to concentration levels, whereas relative uncertainty is anti-correlated, but more weakly (37%).

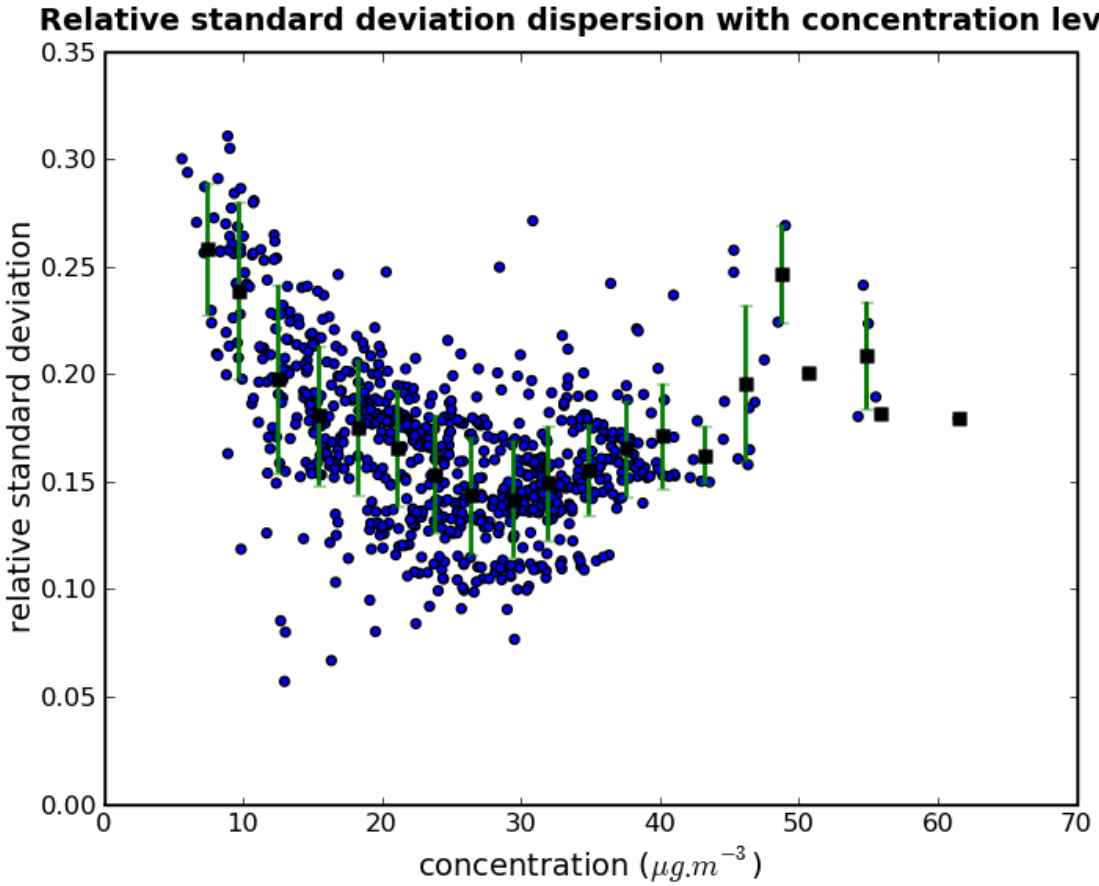

Figure 12: Relative uncertainty dispersion.

Absolute uncertainty tends to increase with the concentration level. The standard deviation of absolute uncertainty with concentration level is 3.3 $\mu g.m^{-3}$, whereas its standard deviation with space is only 0.66 $\mu g.m^{-3}$.

The absolute uncertainty for PM_{10} over urban areas is then mainly driven by the concentration level.

On the contrary, there is no clear tendency between relative uncertainty and concentration level. The relative uncertainty standard deviation with the concentration level and space are respectively 0.2% and 0.3%. Thus the relative uncertainty for PM_{10} over urban areas depends not only by the concentration level but also by the urban area.

5.3 Sensitivity analysis

The purpose of this part is to list the most sensitive parameters of the Chimere model with respect to O_3 and PM_{10} concentrations over urban areas. Such parameters are said illustrative.

Each parameter is allocated one weight coming with its standard deviation.
They are derived according to the methodology detailed in section 2.3, in which each parameter is assigned a weight. The greater the weight the more sensitive the parameter. Each weight has a standard deviation, if this one exceeds half of the weight value, the parameter is discarded.

5.3.1 Ozone

Figure 13 depicts the weights of illustrative parameters for O_3. As an example, the weight of parameter ``LateralBoundary_O3'' (around 50 $\mu g.m^{-3}$) can be interpreted as follows : an 10% increase in O_3 lateral boundaries implies an enhancement in O_3 concentration of 50×0.1 = 5 $\mu g.m^{-3}$. In the same way, a 20% increase in deposition velocities produces a reduction in O_3 concentration of 2.5×0.2 = 5 $\mu g.m^{-3}$

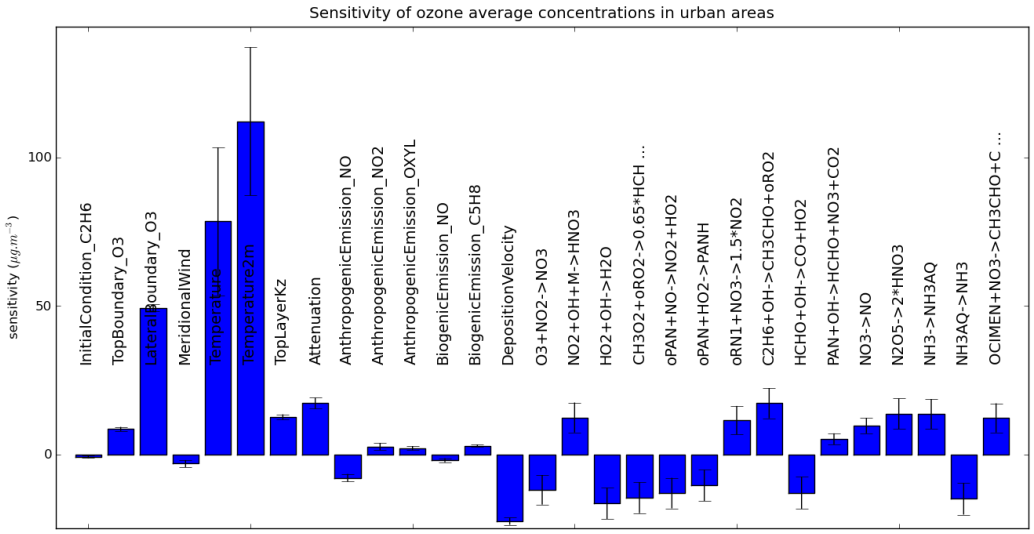

Figure 13: Illustrative parameters for concentrations over urban areas.

Among illustrative parameters, the temperature appears to be the most sensitive for the O_3 average concentration over urban areas. Lateral boundaries have also a significant positive impact, which may be enhanced by the fact that some of the highlighted urban areas are close to the domain boundaries.
That is to note emissions have only a limited impact, still beneath chemical reaction rates.

5.3.2 Particles

Figure 14 depicts the weights of illustrative parameters for PM_{10}.

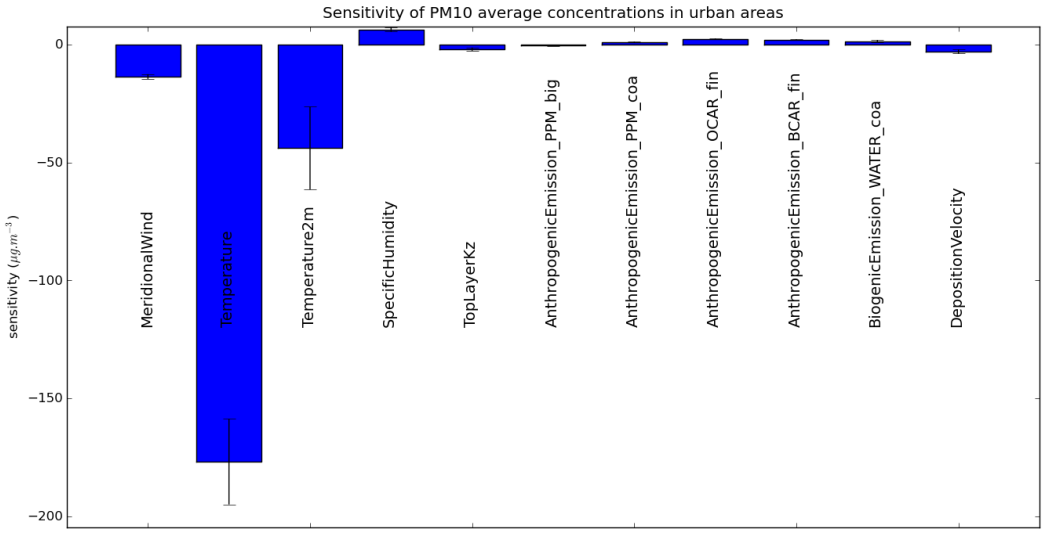

Figure 14: Illustrative parameters for concentrations over urban areas.

As for O_3, temperature still plays an important role in the PM_{10} concentration average over urban areas. An 1% increase in temperature will reduce the PM_{10} concentration by at most 200 $\times$ 0.01 = 2 $\mu g.m^{-3}$.

The sensitivity of remaining parameters cannot be clearly seen in figure 14, we detail them in figure 15.

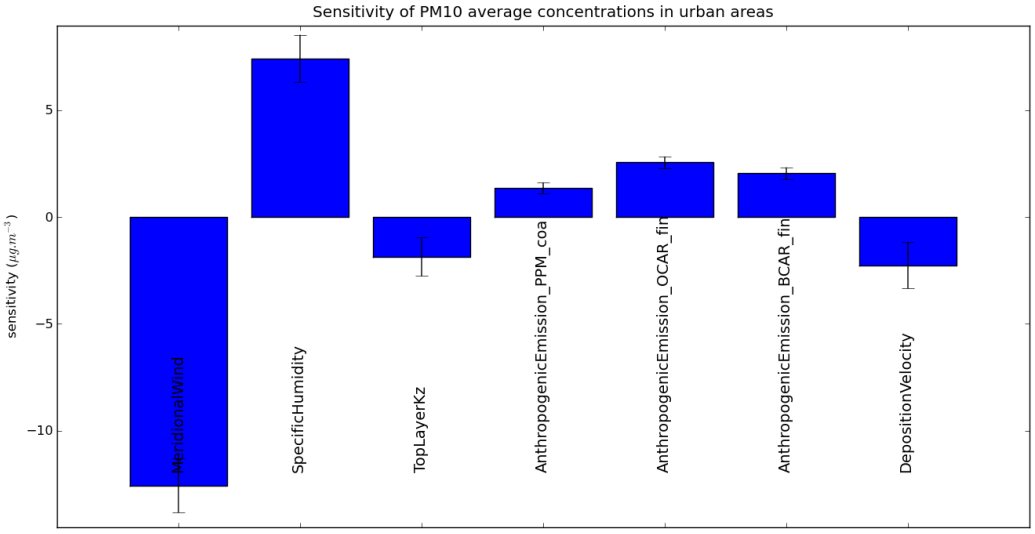

Figure 15: Illustrative parameters for concentrations over urban areas (continued).

One may recognize the positive sensitivity of black and organic carbon emissions, which are generally enhanced over urban areas, as well as the negative sensitivity of particle deposition velocities.

6 Conclusion

In this study, the uncertainty of O_3 in summer and PM_{10} in winter over urban areas has been addressed.

The average absolute and relative uncertainty for O_3 are respectively 16 $\mu g.m^{-3}$ and 21%. Relative uncertainty is mainly driven by the concentration level, decreasing with it, so that relative uncertainty is the lowest on peaks. It doest not change significantly between urban areas.

The average absolute and relative uncertainty for PM_{10} concentrations are respectively 4 $\mu g.m^{-3}$ and 17%. Conversely to O_3, relative uncertainty depends not only on concentration level, slightly reduced on high pollution events, but also on urban area.

According to the sensitivity analysis, notorious illustrative parameters for both pollutants are temperature and deposition velocities. Illustrative parameters peculiar to O_3 concentrations are boundary conditions and chemical reaction rates, whereas those peculiar to PM_{10} concentrations are fine carbon emissions and specific humidity.

The large influence of temperature and boundary conditions on ozone and PM10 concentrations confirm that the impact of emission projections has to be assessed in the context of global changes.

Results obtained so far have yet to be questioned. Indeed, how representative is the estimated uncertainty with respect to the true model uncertainty ? The quality of estimated uncertainty depends not only on the accuracy reached by the Monte Carlo process, but also on how relevant are the PDFs chosen for input parameters.

We refer to the INERIS report [2] for a detailed discussion about the quality of the estimated uncertainty. In view that not not all parameters could be perturbed (e.g. numerical schemes) and that the uncertainty of some input parameters is still poorly known, current estimations should be taken as bottom limits of uncertainties, especially for particles.

Acknowledgements

This work was partly funded by the french Ministry in charge of Ecology (MEEDDM) and the EU LIFE project EC4MACS.

References

[1] Beekmann, M. and Derognat, C. Monte Carlo uncertainty analysis of a regional-scale transport chemistry model constrained by measurements from the Atmospheric Pollution Over the PAris Area (ESQUIF) campaign. *Journal of Geophysical Research*, 108:8559-8576, 2003.

[2] Debry, E. and Malherbe, L. and Honoré, C. and Bessagnet, B. and Rouïl, L. BCRD Incertitudes : Intégration probabiliste pour l'assimilation de données d'observation dans les modèles de qualité de l'air. Rapport final. Technical report, DRC-10-71769-02091A, INERIS, 2010.

[3] Hanna, S.R. and Chang, J.C. and Fernau, M.E. Monte Carlo estimates uncertainties in predictions by a photochemical grid model (UAM-IV) due to uncertainties in input variables. *Atmospheric Environment*, 32:3619-3628, 1998.

[4] Hanna, S.R. and Lu, Z. and Frey, H.C. and Wheeler, N. and Vukovich, J. and Arunachalam, S. and Fernau, M. and Hansen, D.A. Uncertainties in predicted ozone concentrations due to input uncertainties for the UAM-V photochemical grid model applied to the July 1995 OTAG domain. *Atmospheric Environment*, 35:891-903, 2001.

[5] Honoré, C. and Rouïl, L. and Malherbe, L. and Bessagnet, B. and Vautard, R. and Poisson, N. and Colosio, J. Le système Prev'Air : cartographie et prévision de la qualité de l'air à grande échelle en Europe. *Environnement, Risques et Santé*, 3(3):156-64, 2004.

[6] Mallet, V. and Quélo, D. and Sportisse, B. and Ahmed, M. and Debry, E. and Korsakissok, I. and Wu, L. Roustan, Y. and Sartelet, K. and Tombette, M. and Foudhil, H. technical Note : The air quality modeling system Polyphemus. *Atmospheric Chemistry and Physics*, 7(20):5479-5487, 2007.

[7] Romanowicz, R. and Higson, H. and Teasdale, I. Bayesian uncertainty estimation methodology applied to air pollution modelling. *Environmetrics*, 11:351-371, 2000.

[8] Sullivan, D.A. and Holdsworth, M.T. and Hlinka, D.J. Monte Carlo-based dispersion modeling of off-gassing releases from the fumigant metam-sodium for determining distances to exposure endpoints. *Atmospheric Environment*, 38:2471-2481, 2004.